SAND2020-8249J

Liquid-vapor coexistence and critical point of Mg_2SiO_4 from *ab-initio* simulations

Joshua P. Townsend[1], **Gil Shohet**[2], **Kyle R. Cochrane**[1]

[1]High Energy Density Physics Theory, Sandia National Laboratories, Albuquerque, NM, 87185, USA
[2]Department of Aeronautics & Astronautics, Stanford University, Stanford, CA, 94305, USA

Key Points:

- Mg_2SiO_4 vaporizes incongruently and produces Mg-poor and O_2, SiO enriched vapor
- Critical point occurs at lower density and temperature than commonly used multi-phase EOS
- Giant impact simulations underestimate amount of supercritical material post-impact

---

Corresponding author: Joshua P. Townsend, `jptowns@sandia.gov`

Sandia National Laboratories is a multimission laboratory managed and operated by National Technology & Engineering Solutions of Sandia, LLC, a wholly owned subsidiary of Honeywell International Inc., for the U.S. Department of Energy's National Nuclear Security Administration under contract DE-NA0003525.

Abstract

Hypervelocity impact-driven vaporization is characteristic of late-stage planet formation. Yet the behavior and properties of liquid-vapor mixtures of planetary materials of interest are typically unknown. Multiphase equations of state used in hydrodynamic simulations of planet impacts therefore lack reliable data for this important phenomenon. Here, we present the first constraints on the liquid-vapor critical point and coexistence phase boundary of Mg_2SiO_4 computed from *ab-initio* molecular dynamics simulations. We found that the vapor is depleted in magnesium and enriched in silica and oxygen, while the coexisting liquid is enriched in magnesium and depleted in oxygen, from which we infer vaporization is incongruent. The critical point was estimated from an equation of state fit to the data. The results are in line with recent calculations of $MgSiO_3$ and together confirm that extant multiphase EOS models used in planetary accretion modeling significantly underestimate the amount of supercritical material post-impact.

1 Introduction

Planets grow by accretion in which successive collisions of smaller bodies produce large ones. The characteristic impact velocity for an Earth-mass planet is on the order of 10 km/s, and such impacts generate significant amounts of hot liquid and vapor [*Cuk and Stewart*, 2012; *Canup et al.*, 2013; *Nakajima and Stevenson*, 2014; *Lock and Stewart*, 2017]. Beyond the Solar System, large planet impact events have been inferred from astronomical observations of planets orbiting distant stars [*Meng et al.*, 2014]. Therefore, the low-density and high-temperature properties of common planetary materials like silicates and metals are of considerable interest to those studying planet formation across a broad range of initial conditions.

Magnesium silicate Mg_2SiO_4 is ubiquitous in the upper mantle of the Earth and other terrestrial planets as well as pre-planetary and planetary nebulae elsewhere in the galaxy [*Justtanont et al.*, 1992; *de Vries et al.*, 2015]. In hydrodynamic simulations of giant-impact events a multiphase equation of state (EOS) provides closure for mass, momentum, and energy conservation relations, but both experimental data and theoretical models for low density high temperature Mg_2SiO_4 are lacking. Indeed, to-date there exist no experimental thermodynamic data of the critical behavior for any magnesium silicate system. In the absence of any constraints from theory or experiment, multiphase EOS models typically resort to overly simplistic coexistence models and therefore have limited accuracy and may not produce quantitative predictions.

In this Letter, we report the results of a series of *ab-initio* density functional theory (DFT) based molecular dynamics (DFTMD) calculations of Mg_2SiO_4 that span liquid and vapor states (section 2.1 & 3.1). We show that vaporization occurs incongruently and that the chemical composition of the coexisting liquid and vapor is sensitive to the bulk density and temperature (section 3.1). We determine the critical point from an EOS model fit to the pressure-density-temperature states compiled from DFTMD calculations (section 2.2 & 3.2). The rest of the coexistence curve was determined from a fit to an analytic model for the phase boundary. We examine the sensitivity of the estimated critical point to finite size effects and show the results from 224 atom calculations give reasonable estimates of the critical point in the thermodynamic limit. We find that the critical point is substantially different than those used in some previous hydrodynamic simulations of giant impacts, and conclude that those simulations both underestimate the amount of supercritical material, and over-estimate the thermodynamic span of liquid-vapor coexistence post-impact (section 4).

2 Methods

2.1 Molecular dynamics calculations

The gold-standard for computations of critical points is the Gibbs-ensemble Monte Carlo (GEMC) method, in which the equilibrium thermodynamic properties of coexisting vapor and liquid are simulated [*Panagiotopoulos*, 1987]. However, the limitations of this method when applied to multicomponent systems motivates an exploration of alternatives for investigating critical behavior in complex materials. This is especially important for systems in which vaporization may occur incongruently, as expected for multicomponent systems like silicates and other planetary materials. An Alternative to GEMC is molecular dynamics, in which the dynamics of the nuclei are simulated. Molecular dynamics methods have been used to investigate liquid, vapor, coexistence and critical behavior of both single and multicomponent materials with success [*Guissani and Guillot*, 1993; *Kresse and Hafner*, 1997; *de Koker et al.*, 2009; *Desjarlais*, 2009; *Faussurier et al.*, 2009; *Ghosh and Karki*; *Xiao and Stixrude*, 2018].

The goal of this study was to determine the liquid-vapor critical point and coexistence phase boundaries of Mg_2SiO_4 from *ab-initio* DFTMD calculations. To accomplish those goals we carried out a series of DFTMD calculations on supercells spanning 5500-7500 K and 0.22-1.50 g/cm^3, or about 16-2 times expanded with respect to forsterite at ambient conditions. All DFTMD calculations were performed using the `VASP` code (version 5.4.1), an implementation of Kohn-Sham density functional theory (DFT) using a plane-wave basis, projector-augmented-wave pseudopotentials, and periodic boundary conditions [*Kresse and Hafner*, 1993, 1994; *Kresse and Furthmüller*, 1996]. The irreducible Brillouin zone for those supercells was sampled at the Baldereschi mean value (k=(0.25, 0.25, 0.25)), and the electronic occupations were populated using a Fermi-Dirac distribution according to the Mermin finite temperature formulation of DFT [*Mermin*, 1965]. The exchange and correlation contributions to the energy were computed using the PBE generalized gradient approximation [*Perdew et al.*, 1996]. The VASP PAW pseudopotentials were used with a plane wave energy cutoff of 800 eV, which provided converged values of the stress tensor at the lowest density we studied. Because the temperatures and densities considered in our study were not too high, we used a magnesium pseudopotential with a $3s^2$ valence configuration, while that of silicon and oxygen were $3s^2 3p^2$, and $2s^2 2p^4$, respectively. All calculations were performed on cubic simulation cells within the NVT ensemble using a velocity-scaling thermostat and a 1 femtosecond timestep for the nuclear motion.

A system at a critical point is characterized by density fluctuations at all length scales. This is problematic from the standpoint of atomistic simulations, which are necessarily finite. As a consequence, finite size effects were a principal concern. We therefore performed DFTMD calculations in supercells containing 28, 56, 112, and 224 atoms in order to quantify the finite size errors associated with the critical point density, temperature, and pressure. Equilibration time of the system near the critical point was another concern. Typically, we found that around 2-5 ps of simulated time was sufficient to equilibrate the system, and that a further 4-5 ps of simulated time provided accurate pressures. Equilibration was checked in a few cases by allowing some simulations to run for up to 100 ps in the 28 and 56 atom supercells.

2.2 EOS model and critical point estimation

The simplest equation of state (EOS) with a critical point is cubic in the density:

$$P(\rho, T) = (a_0 + a_1 T)\rho + (b_0 + b_1 T)\rho^2 + (c_0 + c_1 T)\rho^3 \tag{1}$$

where P, ρ, T are pressure, density, and temperature, respectively. Eqn. 1 is a generalized virial equation of state and was selected for its flexibility and generality in describing both liquids and gases. Cubic equations of state are commonly used to describe critical phenomena of a wide class of materials [*Wong and Sandler*, 1992; *Guissani and Guillot*, 1993; *Valderrama*, 2003; *Faussurier et al.*, 2009]. Regardless of the underlying EOS model, the critical point satisfies:

$$\left(\frac{\partial P}{\partial \rho}\right)_T = \left(\frac{\partial^2 P}{\partial \rho^2}\right)_T = 0 \tag{2}$$

which corresponds to the statement that the first order transition from liquid to vapor becomes second order at the critical point [*Hansen and McDonald*, 1990]. These criteria together with the EOS model yield an analytic solution for the critical point:

$$T_C = \frac{-B \pm \sqrt{B^2 - 4AC}}{2A} \tag{3}$$

$$\rho_C = -\frac{b(T_C)}{3c(T_C)} \tag{4}$$

$$P_C = P(\rho_C, T_C) \tag{5}$$

with $A = a_1 c_1 - \frac{1}{3} b_1^2$, $B = a_0 c_1 + a_1 c_0 - \frac{2}{3} b_0 b_1$, and $C = a_0 c_0 - \frac{1}{3} b_0^2$.

Our strategy is then straightforward: Run DFTMD simulations on a grid of ρ, T points for systems of different sizes, then fit the subsequent $P(\rho, T)$ data to the EOS model from which the critical point is obtained for each system. The DFTMD data with best fit EOS models and critical points for all systems studied are provided in the supplementary materials in fig. S1 and table S1. The appeal of this approach is its simplicity. Our estimate of the critical point does not depend on detailed knowledge of the internal distribution of liquid and vapor in the simulation cell, rather we require only $P(\rho, T)$, which is an easily quantifiable bulk thermodynamic property which converges rapidly with respect to the simulation time.

3 Results

3.1 Chemical and structural properties in the vicinity of the critical point

Direct inspection of the DFTMD trajectories indicates that the calculations spanned pure liquid, coexisting liquid and vapor, and vapor states, as shown in fig. 1. Due to the chemical complexity of Mg_2SiO_4, we did not expect to be able to unambiguously label, in general, any particular collection of atoms as belonging to either liquid or vapor. However, we found that the most abundant species were easily identifiable small molecules such as O, O_2, SiO, SiO_2, MgO, and Mg, which clearly composed the vapor phase. The speciation of these small molecules for several isotherms is shown in fig. 2 and the corresponding bond lifetimes are shown in fig. S3. At intermediate densities the system tended to segregate into long-lived large globs of liquid and a variety of vapor species, and at the highest density we studied, 1.50 g/cm^3, we find that the system is nearly completely liquid with a small amount of transient molecular and atomic oxygen.

Broadly, where liquid and vapor coexisted, we found that the liquid was enriched in magnesium and depleted in silica and oxygen as compared to the vapor, which was enriched in oxygen and silica and depleted in magnesium. For example, at 6250 K and 0.50 g/cm^3 the composition

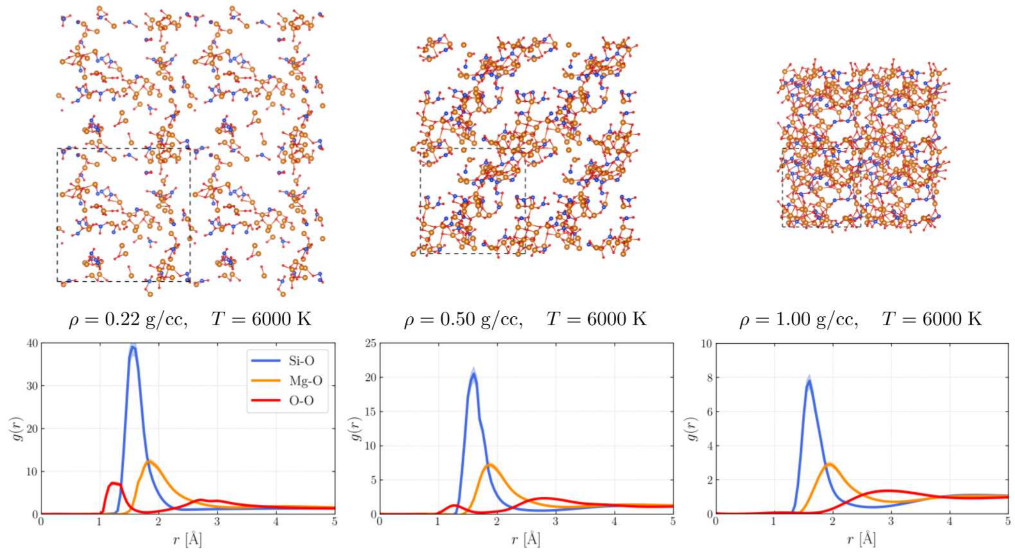

Figure 1. Selected snapshots of DFTMD trajectories (top) for the 224-atom system for various densities on 6000 K isotherm, and corresponding spherically averaged pair distribution functions, $g(r)$ (bottom). As the system is expanded coexistence of liquid and vapor are clearly observed. Magnesium, silicon, and oxygen are represented by orange, blue, and red spheres, respectively. The snapshots have been tiled to more clearly show the large-scale structure of the system (actual simulation regions marked with dashed lines).

of the liquid is $Mg_{61.8\pm0.2}Si_{29.6\pm0.2}O_{116.0\pm0.5}$, or normalized to silicon: $Mg_{2.1\pm0.1}Si_{1.00}O_{3.9\pm0.2}$. Similarly, for the vapor we found a composition of $Mg_{2.2\pm0.2}Si_{2.4\pm0.2}O_{12.0\pm0.5}$, or normalized to silicon: $Mg_{0.9\pm0.1}Si_{1.0}O_{5.1\pm0.2}$. Evidently, the liquid retained a composition of nearly stoichiometric Mg_2SiO_4, while that of the vapor was somewhat different, in line with a recent study of $MgSiO_3$ at similar conditions [*Xiao and Stixrude*, 2018]. We also found that the onset of vaporization at all temperatures was characterized by the appearance of molecular and atomic oxygen, the latter of which, as expected, was more abundant at higher temperatures. The results suggest that vaporization of Mg_2SiO_4 occurs incongruently (*i.e.* that the compositions of the coexisting liquid and vapor are different), similar to recents investigations of the critical behavior of other silicates [*Kraus et al.*, 2012; *Xiao and Stixrude*, 2018; *Connolly*, 2016]. Although there are no experimental data on the critical behavior of Mg_2SiO_4, comparison of our results with experimental data on vaporization at lower pressures suggest that vaporization is complex; at lower pressure and temperature boiling of Mg_2SiO_4 was previously reported to occur congruently [*Nagahara et al.*, 1994]. More recent experiments on iron-bearing olivine suggest incongruent vaporization [*Costa et al.*, 2017].

3.2 Critical Point Estimation & Uncertainty Quantification

The critical point was computed analytically from a fit of the EOS given in eqn. 1 to the $P(\rho, T)$ points from the DFTMD calculations. The 224 atom results are most representative of the properties of the system in the thermodynamic limit, and so we report in the main text those results unless otherwise indicated. The best-fit critical point values obtained are: $\rho_c = 0.52 \pm 0.03$ g/cm^3, $T_c = 6240 \pm 200$ K, and $P_c = 1.3 \pm 0.2$ kbar. The data and corresponding best-fit EOS are shown in fig. 3. In the coexistence region isotherms below the critical point clearly display van der Waals loops. In the thermodynamic limit such curvature is unphysical because it implies a negative compressibility and an imaginary sound speed. However, from the standpoint of atomistic simulation, every point on the isotherm is stable and the curvature is in part due to finite size-effects [*Binder et al.*, 2012]. This effect is readily observed from the results of the simulations by comparing the curvature of the isotherms obtained from the different sized simulation cells: isotherms obtained from simulations on the smaller cells have more pronounced curvature in the coexistence region than those obtained from larger cells (fig. S1). Essentially, the result is that for the data presented here, the local maxima and minima in the isotherms in the coexistence region do not correspond to spinodal decomposition.

With one point on the liquid-vapor phase boundary in hand, we estimated the limits of co-existence below the critical point via the familiar Maxwell equal-area construction [*Callen*, 2006]. Famously, renormalization group theory applied to critical behavior in the 3d Ising model gives an analytic form for the phase boundaries for the vapor and liquid sides of the vapor dome:

$$\rho_v = \rho_c - \frac{1}{2}\left(C_1 x^{\beta} + C_2 x^{\beta+\Delta}\right) + C_3 x \tag{6}$$

$$\rho_l = \rho_c + \frac{1}{2}\left(C_1 x^{\beta} + C_2 x^{\beta+\Delta}\right) + C_3 x \tag{7}$$

with $x \equiv \left(1 - \frac{T}{T_C}\right)$, $\beta = 0.325$, and $\Delta = \frac{1}{2}$ [*Pathria and Beale*, 2011; *Hansen and McDonald*, 1990]. Recently this approach has been employed by *Xiao and Stixrude* [2018] to describe coexistence in $MgSiO_3$. The phase boundary estimates from the Maxwell construction and subsequent analytic fit for the 112 and 224 atom cells are shown in fig. 3.2. As expected, the vapor-side of the coexistence region is poorly resolved, even in the largest simulation cell we studied. This is due to the finite size of the simulations and because the isotherms are extrapolated below 0.22 g/cm^3. However, the liquid side of the dome shows smaller finite size effects resulting in improved agreement between systems. For that reason, only the points closest to the critical point on the vapor-side of the critical point were included in the analytic fit, from which we obtained C_1=1.23 ± 0.08, C_2=2.28 ± 0.35, C_3=1.24 ± 0.14.

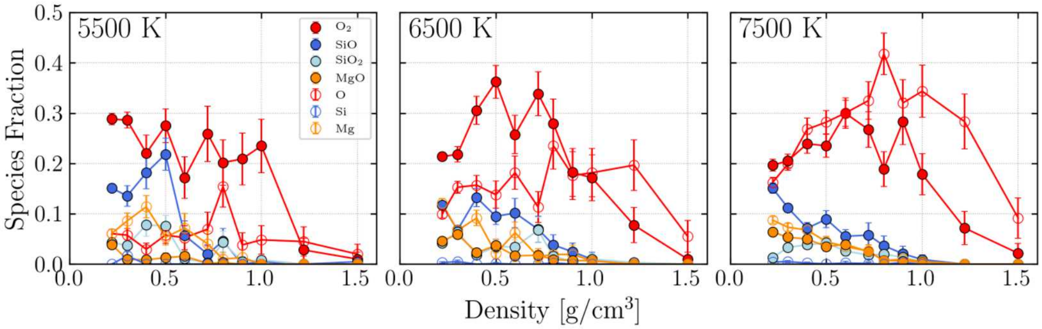

Figure 2. Abundance of selected light species in the vapor along 5500 K, 6500 K, and 7500 K isotherms. The species fraction is the number of molecules of a particular type divided by the total number of molecules in the cell.

Finally, it was important to compare the estimated critical points for systems of different sizes in order to investigate the finite size effects associated with our estimation of the critical point. We find that the critical points for the 112-atom and 224-atom cells are within their mutual uncertainties, as shown in fig. 4. Combining the results from the 28-, 56-, 112-, and 224-atom cells and extrapolating the critical point parameters yields an estimate of the critical point in the thermodynamic limit (shown in fig. S2): $\rho_c^{extrap} = 0.51 \pm 0.01$ g/cm^3, $T_C^{extrap} = 6110 \pm 26$ K, and $P_c^{extrap} = 1.14 \pm 0.09$ kbar, which is within the uncertainties of the results from the 224 atom cell. We conclude that the finite size effects in the critical point estimate in the 224 atom cell are small.

4 Discussion & Conclusions

The major result of the present study establishes a first estimate of the critical behavior of Mg_2SiO_4, the most abundant phase in the Earth's outermost layers, as well as the Moon. We find that the critical point and liquid-vapor phase boundary estimated from DFT-MD calculations differs substantially from those in commonly used multiphase EOS models of giant impact and accretion simulations (*cf. Canup* [2012]; *Cuk and Stewart* [2012]; *Nakajima and Stevenson* [2014]; *Lock and Stewart* [2017]). In the ANEOS model for forsterite, for example the critical point is at 1.68 g/cm^3, 8800 K, and 10 kbar, while our results suggest a critical point at 0.52 g/cm^3, 6230 K, and 1.22 kbar [*Stewart et al.*, 2020]. This is significant as is suggests that nearly all accretionary collisions produce some amount of vaporization [*Davies et al.*, 2020]. In larger collisions characteristic of late-stage accretion of Earth-sized planets, impact velocities often exceed 10 km/s [*Greenberg et al.*, 1978]. The heat and entropy liberated from such an event typically results in prodigious amounts of hot liquid,

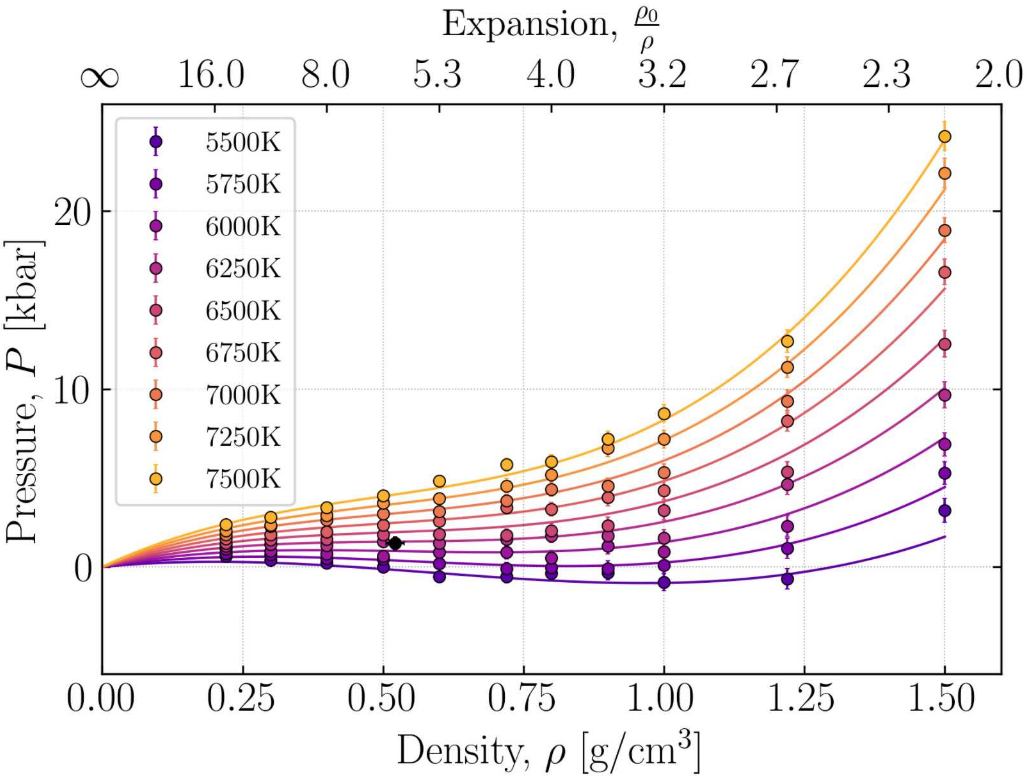

181 **Figure 3.** EOS fit (lines) to DFTMD results (points) of 224 atom system with critical point (black circle).

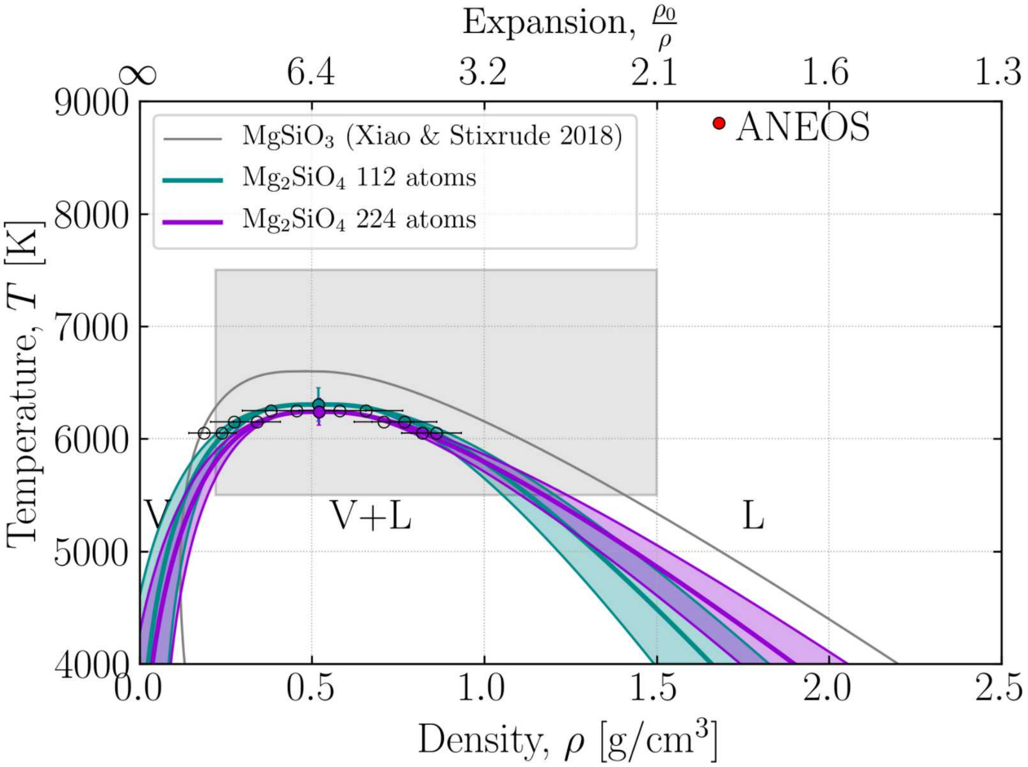

Figure 4. (L)iquid-(V)apor phase boundaries obtained from Maxwell constructions from 224 and 112-atom data sets (right). Filled circles mark critical points obtained from EOS. Unfilled circles mark phase boundary estimates from the Maxwell constructions. Lines and shaded regions show phase boundary and 1σ confidence interval. The grey box shows the simulation domain. The red point marks the location of the critical point in the tabulated EOS models used in some hydrodynamic simulations of giant impacts [*Stewart et al.*, 2019].

vapor, and supercritical fluid immediately post-impact [*Lock and Stewart*, 2017]. How the system evolves post-impact would obviously influence the compositions of any eventual planet or moon. Therefore, hydrodynamic simulations that rely on incorrect EOS models will underestimate the quantity of supercritical material, and overestimate the quantity of distinct liquid and vapor phases, which might subsequently influence the chemical compositions of the resulting bodies [*Stewart et al.*, 2020].

There are several limitations in the present study which suggest possible avenues of future research. As with all DFT calculations, the choice of exchange correlation functional introduces a systematic bias in the results. Although we expect this bias to be relatively small for the problem studied here, the choice of functional on critical point parameters is an interesting topic for future study. It is notable that at intermediate densities the atomic fraction of the cell that is composed of vapor is only about 16 out of 224 atoms, about 7%, so larger simulations may better resolve the speciation in the vapor. Similarly, the vapor side of the Maxwell construction would likely be better resolved in much larger systems which may soon be possible through the use of sophisticated classical interatomic potentials such as the recently developed SNAP [*Wood and Thompson*, 2018].

However, the main limitation of both this and previous work on silicates is the assumption of single-component-like critical behavior. Although the EOS isotherms of the present study show all the trademark features of single component critical behavior, Mg_2SiO_4 is a multicomponent system, and therefore may not have a single critical point. Despite this assumption, an in-depth study of the critical behavior of SiO_2 by *Connolly* [2016] suggests that the width of the liquid-vapor phase boundary in SiO_2 is relatively narrow and thus is likely smaller than the uncertainties on the densities of the coexisting liquid and vapor from our calculations, as shown in fig. 4. In accordance with other silica-bearing systems studied thus far, the assumption of single component-like critical behavior seems reasonable given the current state of knowledge of these materials, and the capabilities of current hydrodynamic simulation techniques [*Kraus et al.*, 2012; *Connolly*, 2016; *Xiao and Stixrude*, 2018; *Stewart et al.*, 2020].

These limitations aside, the advantage of the present approach is that the estimation of the critical point does not depend on detailed knowledge of the atomic-scale structures in the simulation, but instead on the bulk thermodynamic properties of the mixed system. The fact that the present and previous studies of Mg-bearing silicate systems find remarkably similar critical points despite using entirely independent methods lends confidence to these approaches despite their assumptions.

In summary, the study of the critical behavior of planetary materials offers important constraints on multiphase EOS models needed for accurate studies of planet formation. For the Mg_2SiO_4 system, recent experimental and theoretical studies have led to significant improvements in the EOS in high density, high pressure, high temperature regimes [*Root et al.*, 2018; *Stewart et al.*, 2019]. The present work extends these improvements to low pressure, low density, and moderate temperature.

Acknowledgments

The authors thank Michael P. Desjarlais, Luke Shulenburger, Raymond C. Clay III, and Sarah T. Stewart for many fruitful discussions which greatly improved the quality of this manuscript. G.S. was supported by the DOE SSGF program grant number DE-NA0003864. J.P.T. and K.R.C. acknowledge support from the Z Fundamental Science Program. Sandia National Laboratories is a multimission laboratory managed and operated by National Technology and Engineering Solutions of Sandia, LLC., a wholly owned subsidiary of Honeywell International, Inc., for the U.S. Department of Energy's National Nuclear Security Administration under contract DE-NA0003525. This paper describes objective technical results and analysis. Any subjective views or opinions that might be expressed in the paper do not necessarily represent the views of the U.S. Department of Energy or the United States Government. The data used in this manuscript can be obtained from `https://doi.org/10.5281/zenodo.3970968`.

References

Binder, K., B. J. Block, P. Virnau, and A. Tröster (2012), Beyond the van der waals loop: What can be learned from simulating lennard-jones fluids inside the region of phase coexistence, *American Journal of Physics*, *80*, 1099–1109, doi:10.1119/1.4754020.

Callen, H. B. (2006), *Thermodynamics & an Intro. to Thermostatistics*, John Wiley & Sons.

Canup, R., A. Barr, and D. Crawford (2013), Lunar-forming impacts: High-resolution sph and amr-cth simulations, *Icarus*, *222*, 200 – 219, doi:https://doi.org/10.1016/j.icarus.2012.10.011.

Canup, R. M. (2012), Forming a moon with an earth-like composition via a giant impact, *Science*, *338*, 1052.

Connolly, J. A. (2016), Liquid-vapor phase relations in the si-o system: A calorically constrained van der waals-type model, *Journal of Geophysical Research: Planets*, *121*, 1641–1666, doi:10.1002/2016JE005059.

Costa, G. C., N. S. Jacobson, and B. F. Jr. (2017), Vaporization and thermodynamics of forsterite-rich olivine and some implications for silicate atmospheres of hot rocky exoplanets, *Icarus*, *289*, 42 – 55, doi:https://doi.org/10.1016/j.icarus.2017.02.006.

Cuk, M., and S. T. Stewart (2012), Making the moon from a fast-spinning earth: A giant impact followed by resonant despinning, *Science*, *338*, 1047.

Davies, E. J., P. J. Carter, S. Root, R. G. Kraus, D. K. Spaulding, S. T. Stewart, and S. B. Jacobsen (2020), Silicate melting and vaporization during rocky planet formation, *Journal of Geophysical Research: Planets*, *125*(2), e2019JE006,227, doi:10.1029/2019JE006227.

de Koker, N. P., L. Stixrude, and B. B. Karki (2009), Thermodynamics, structure, dynamics, and freezing of mg2sio4 liquid at high pressure, *Geochimica et Cosmochimica Acta*, *72*, 1427–1441, doi:10.1016/j.gca.2007.12.019.

de Vries, B. L., K. Maaskant, M. Min, R. Lombaert, L. Waters, and J. Blommaert (2015), Micron-sized forsterite grains in the pre-planetary nebula of iras 17150- 3224-searching for clues to the mysterious evolution of massive agb stars, *Astronomy & Astrophysics*, *576*, A98, doi:10.1051/0004-6361/201424843.

Desjarlais, M. P. (2009), Quantum molecular dynamics simulations for generating equation of state data, *AIP Conference Proceedings*, *1161*, 32–38, doi:10.1063/1.3241205.

Faussurier, G., C. Blancard, and P. L. Silvestrelli (2009), Evaluation of aluminum critical point using an ab initio variational approach, *Phys. Rev. B*, *79*, 134,202, doi:10.1103/PhysRevB.79.134202.

Ghosh, D. B., and B. B. Karki ().

Greenberg, R., J. F. Wacker, W. K. Hartmann, and C. R. Chapman (1978), Planetesimals to planets: Numerical simulation of collisional evolution, *Icarus*, *35*, 1 – 26.

Guissani, Y., and B. Guillot (1993), A computer simulation study of the liquid–vapor coexistence curve of water, *The Journal of Chemical Physics*, *98*(10), 8221–8235, doi:10.1063/1.464527.

Hansen, J.-P., and I. R. McDonald (1990), *Theory of simple liquids*, Elsevier.

Justtanont, K., M. J. Barlow, C. J. Skinner, and A. G. G. M. Tielens (1992), The Nature of Dust around the Post–Asymptotic Giant Branch Objects HD 161796 and HD 179821, *The Astrophysical Journal*, *392*, L75, doi:10.1086/186429.

Kraus, R. G., S. T. Stewart, D. C. Swift, C. A. Bolme, R. F. Smith, S. Hamel, B. D. Hammel, D. K. Spaulding, D. G. Hicks, J. H. Eggert, and G. W. Collins (2012), Shock vaporization of silica and the thermodynamics of planetary impact events, *J. Geophys. Res. - Planet*, *117*, E09,009, doi:10.1029/2012JE004082.

Kresse, G., and J. Furthmüller (1996), Efficient iterative schemes for ab initio total-energy calculations using a plane-wave basis set, *Phys. Rev. B*, *54*, 11,169.

Kresse, G., and J. Hafner (1993), Ab initio molecular dynamics for liquid metals, *Phys. Rev. B*, *47*, R558.

Kresse, G., and J. Hafner (1994), Ab initio molecular-dynamics simulation of the liquid-metal-amorphous-semiconductor transition in germanium, *Phys. Rev. B*, *49*, 14,251.

Kresse, G., and J. Hafner (1997), Ab initio simulation of the metal/nonmetal transition in expanded fluid mercury, *Phys. Rev. B*, *55*, 7539–7548, doi:10.1103/PhysRevB.55.7539.

Lock, S. J., and S. T. Stewart (2017), The structure of terrestrial bodies: Impact heating, corotation limits, and synestias, *Journal of Geophysical Research: Planets*, *122*, 950–982, doi:10.1002/2016JE005239.

Meng, H. Y. A., K. Y. L. Su, G. H. Rieke, D. J. Stevenson, P. Plavchan, W. Rujopakarn, C. M. Lisse, S. Poshyachinda, and D. E. Reichart (2014), Large impacts around a solar-analog star in the era of terrestrial planet formation, *Science*, *345*(6200), 1032–1035, doi:10.1126/science.1255153.

Mermin, N. D. (1965), Properties of the inhomogeneous electron gas, *Phys. Rev.*, *137*, A1441.

Nagahara, H., I. Kushiro, and B. O. Mysen (1994), Evaporation of olivine: Low pressure phase relations of the olivine system and its implication for the origin of chondritic components in the solar nebula, *Geochimica et Cosmochimica Acta*, *58*, 1951 – 1963, doi:https://doi.org/10.1016/0016-7037(94)90426-X.

Nakajima, M., and D. J. Stevenson (2014), Investigation of the initial state of the moon-forming disk: Bridging sph simulations and hydrostatic models, *Icarus*, *233*, 259 – 267, doi:

https://doi.org/10.1016/j.icarus.2014.01.008.

Panagiotopoulos, A. Z. (1987), Direct determination of phase coexistence properties of fluids by monte carlo simulation in a new ensemble, *Molecular Physics*, *61*, 813–826, doi: 10.1080/00268978700101491.

Pathria, R., and P. Beale (2011), *Statistical Mechanics 3rd ed.*, Academic Press, Boston.

Perdew, J., K. Burke, and M. Ernzerhof (1996), Generalized gradient approximation made simple, *Phys. Rev. Lett.*, *77*, 3865–3868, doi:10.1103/PhysRevLett.77.3865.

Root, S., J. P. Townsend, E. Davies, R. W. Lemke, D. E. Bliss, D. E. Fratanduono, R. G. Kraus, M. Millot, D. K. Spaulding, L. Shulenburger, S. T. Stewart, and S. B. Jacobsen (2018), The principal hugoniot of forsterite to 950 gpa, *Geophysical Research Letters*, *45*, 3865–3872, doi: 10.1029/2017GL076931.

Stewart, S., E. Davies, M. Duncan, S. Lock, S. Root, J. Townsend, R. Kraus, R. Caracas, and S. Jacobsen (2020), The shock physics of giant impacts: Key requirements for the equations of state, *21st Biennial APS Conference on Shock Compression of Condensed Matter (SCCM19)*.

Stewart, S. T., E. J. Davies, M. S. Duncan, S. J. Lock, S. Root, J. P. Townsend, R. G. Kraus, R. Caracas, and S. B. Jacobsen (2019), The shock physics of giant impacts: Key requirements for the equations of state.

Valderrama, J. O. (2003), The state of the cubic equations of state, *Industrial & Engineering Chemistry Research*, *42*(8), 1603–1618, doi:10.1021/ie020447b.

Wong, D. S. H., and S. I. Sandler (1992), A theoretically correct mixing rule for cubic equations of state, *AIChE Journal*, *38*(5), 671–680, doi:10.1002/aic.690380505.

Wood, M. A., and A. P. Thompson (2018), Extending the accuracy of the snap interatomic potential form, *The Journal of Chemical Physics*, *148*, 241,721, doi:10.1063/1.5017641.

Xiao, B., and L. Stixrude (2018), Critical vaporization of mgsio3, *Proceedings of the National Academy of Sciences*, *115*, 5371–5376, doi:10.1073/pnas.1719134115.